CHAPTER 10.A

Amyloid as a ribbon-like micelle

Mateusz Banach[1], **Irena Roterman**[1]
[1]Department of Bioinformatics and Telemedicine, Jagiellonian University—Medical college, Krakow, Poland

Contents

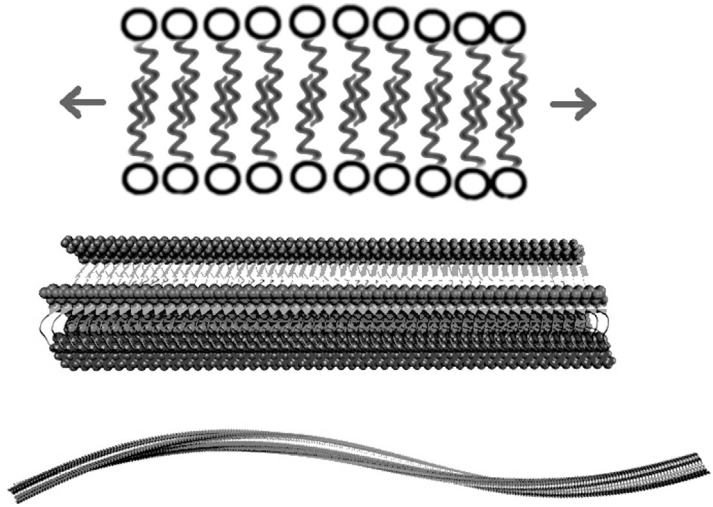

Different scales of ribbon-like micelle presentation visualizing the linear propagation of hydrophilic (white circles) and hydrophobic (black zigzag lines) bands (top). The central picture visualizes the amyloid Aβ(15—40) containing 50 polypeptides. The long fragment of fibril Aβ(15—40) containing 200 peptides (bottom). The

From Globular Proteins to Amyloids
ISBN: 978-0-08-102981-7
https://doi.org/10.1016/B978-0-08-102981-7.00016-6

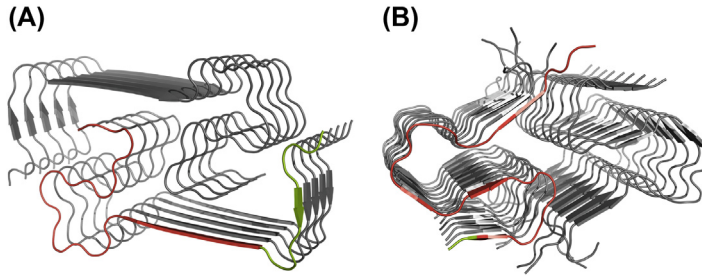

Fig. 10.A.1 3D presentation superfibrils. (A) Aβ(1−40) (2MVX). (B) Aβ(11−42) (5KK3). An example chain in each protein is distinguished from the rest of the complex by red and green colors. Red color marks 11-40 fragments where sequences of the proteins are identical. Conversely, green color denotes fragments where the sequences differ.

structures generated as the multiplication of short fragments available in PDB. The intensity of gray color is proportional to hydrophobicity level.

In this chapter we will discuss the following amyloid proteins:

1. Amyloid Aβ(1−40) peptide with the Osaka mutation (E22Δ) (PDB ID: 2MVX) [1].
2. Amyloid Aβ(11−42) fragment 672−713 −superfibril consisting of Aβ42 molecules, each containing four β-strands in an S-shaped configuration (PDB ID: 5KK3) [2].
3. Prion domain of the fungal prion HET-s in its amyloid form, available in PDB as 2KJ3 [3].

Two of these structures (2MVX and 5KK3) are fragments of the Aβ(1−42) amyloid. Despite substantial sequential similarities (identical sequence at 11−40), they exhibit major conformational differences (Fig. 10.A.1). Both proteins share a common property: they form superfibrils which consist of two dimerized protofibrils each, although with differing symmetry: the structure of 2MVX includes five-chain protofibrils, while in the case of 5KK3 each protofibril is composed of 10 chains.

Amyloid Aβ(1−40) peptide with the Osaka mutation (E22Δ)

The theoretical distribution for Aβ(1−40) (2MVX) (Fig. 10.A.2) accounts for an expected peak at the protein's core. Here, T consists of multiple profiles, characterized by increasing values of hydrophobicity − an

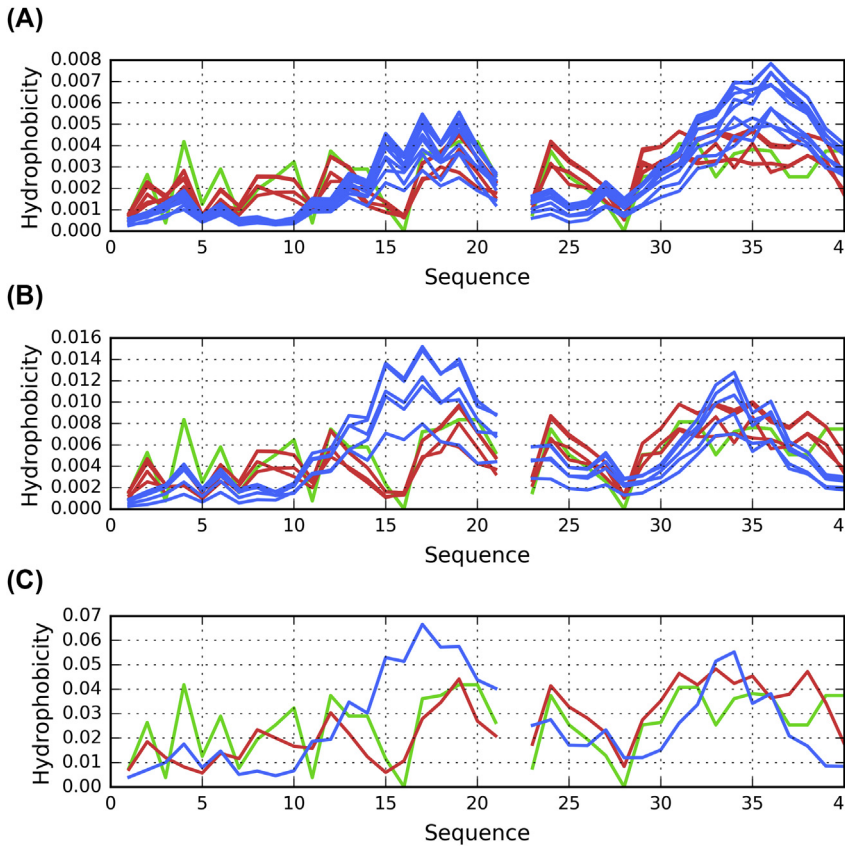

Fig. 10.A.2 Theoretical (T, blue), observed (O, red) and intrinsic (H, green) hydrophobicity distribution profiles for Aβ(1−40) (2MVX). (A) superfibril. (B) protofibril (chains A, B, C, D, E). (C) individual (central) chain of protofibril (C). In each case a Gaussian capsule is constructed specifically for the structural unit undergoing analysis. There is no residue number 22 in the sequence, however there is no gap in the chains within the PDB structure.

effect caused by the variable distance of successive polypeptides from the center of the fibril (where high hydrophobicity is expected).

In contrast, observed (O) distribution plots reveal near-identical values for all internal chains, with only a slight decrease in hydrophobicity in the outlying (edge) chains. If we note that experimentally observed fibrils are capable of unlimited propagation, it follows that these internal chains are representative of the distribution of hydrophobicity which spans the entire fibril. Differences between the theoretical and observed distribution —

particularly concerning the location of hydrophobicity minima and maxima – are stark. Unlike T, where only two peaks are present, the observed distribution resembles a high-frequency sinusoid and comprises five distinct maxima.

Calculation of fuzzy oil drop parameters (Table 10.A.1) shows that both the superfibril and the protofibril exhibit high RD values in both variants

Table 10.A.1 Fuzzy oil drop parameters for Aβ(1–40) (2MVX), computed for superfibril, protofibril and chain C, both as a standalone structure, as part of the protofibril and as part of the superfibril. Values given in bold represent the status interpreted as amyloid seed.

Aβ(1–40) (2MVX)	Fragment	RD		Correlation coefficient		
		T-O-R	T-O-H	HvT	TvO	HvO
Superfibril		0.590	0.592	0.438	0.674	0.727
Chain C in superfibril						
Complete	1–40	0.608	0.620	0.459	0.665	0.784
	1–10	0.663	0.569	0.401	0.216	0.733
	11–16	**0.706**	**0.475**	**−0.420**	**−0.496**	**0.910**
	17–28	0.564	0.527	0.707	0.554	0.927
	29–40	0.853	0.648	0.250	0.298	−0.003
	10–27	0.698	0.646	0.250	0.221	0.886
Chain C in protofibril						
Complete	1–40	0.632	0.666	0.312	0.369	0.784
	1–10	0.554	0.532	0.692	0.333	0.693
	11–16	**0.690**	**0.475**	**−0.413**	**−0.669**	**0.892**
	17–28	0.545	0.526	0.735	0.552	0.923
	29–40	0.816	0.704	0.177	0.688	0.194
	10–27	0.691	0.660	0.162	0.020	0.872
Chain C as individual unit						
Complete	1–40	0.636	0.562	0.295	0.363	0.616
	1–10	0.738	0.541	0.555	−0.287	0.257
	11–16	**0.743**	**0.336**	**−0.464**	**−0.720**	**0.693**
	17–28	0.621	0.413	0.749	0.455	0.822
	29–40	0.797	0.690	0.159	0.611	−0.022
	10–27	0.695	0.507	0.195	0.101	0.697

(T-O-R and T-O-H). Notably, the alignment between O and H is better than between O and R, indicating that formation of the fibril is driven by the intrinsic hydrophobicity of its constituent residues. This view is further supported by high values of HvO, especially when compared to the other two correlation coefficients (even though the dominance of HvO is not overwhelming).

The status of the C chain, which occupies a central position and therefore provides the best representative for a putative "endless" fibril, indicates further deviation from T in favor of H. This conclusion follows from analysis of its RD and correlation coefficients. The RD for T-O-H is below 0.5, however the very large bias in correlation coefficient significantly favoring the relation HvO suggests this interpretation.

Individual chains may be analyzed in the context of their respective super- or protofibrils, but also on their own (i.e. using a 3D Gaussian capsule which is limited to the chain undergoing analysis). In this case, the status of the 11—16 fragment is particularly noteworthy since it exhibits negative HvT and TvO values while its HvO value is particularly high. Negative correlation indicates that the observed distribution is not only discordant from theoretical values, but in fact opposes it, at least to a certain extent. Clearly, intrinsic hydrophobicity has a particularly strong effect on O within this fragment. The remaining fragments (corresponding to each local maximum) also reveal close alignment between the intrinsic and observed distributions of hydrophobicity.

In effect, the following parameters may be regarded as characteristic "markers" of an amyloid structure: high values of RD (both variants), negative values of HvT and TvO, and a strongly positive value of HvO (Fig. 10.A.2 and Table 10.A.1).

The parameters listed in Table 10.A.1 show that the 11—16 fragment is particularly discordant from the monocentric distribution of hydrophobicity. Lys16 is an especially noteworthy residue, since it acts as a "breaker", splitting the expected broad maximum into two shorter (and less hydrophobic) fragments. Given that the same arrangement is replicated in successive chains, we may assume that residue 16 acts as a hydrophilic band interposed between two adjacent hydrophobic bands. This linear pattern emerges as a result of clustering between identical chains along the fibril's axis of propagation. As a result, the fibril as a whole is dominated by alternating bands of high and low hydrophobicity which depend upon the intrinsic properties of individual residues (Fig. 10.A.3).

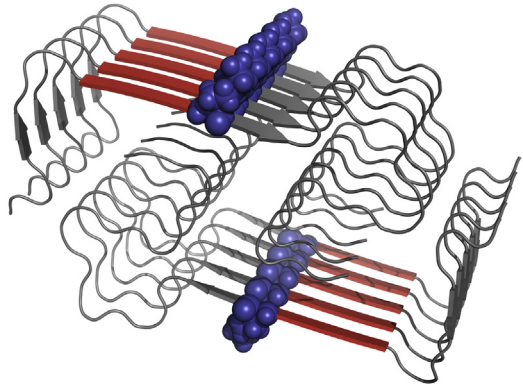

Fig. 10.A.3 3D presentation of Aβ(1−40) (2MVX), with 11−16 fragment in each chain highlighted in red. Lys16, located at the end of this fragment, is shown as blue spheres.

Aβ(11−42) amyloid

When a similar analysis is performed for the Aβ(11−42) amyloid (5KK3), it turns out that the aforementioned criteria are met by the superfibril, by each protofibril as well as by individual chains. In this case, however, the fragment which satisfies the stated conditions is the one at 24−28 (Fig. 10.A.4, Table 10.A.2). A local maximum is present where the theoretical model expects a local minimum (if the molecule were to adopt a globular conformation). This also implies that a locally hydrophobic band is exposed to the outside environment − an unfavorable condition, particularly if the band stretches along the entire axis of the fibril. It is important to recall that each local maximum observed in an individual chain translates into a long band, and that the overall distribution of hydrophobicity in the amyloid fibril is very much unlike the distribution predicted for a globular protein (Fig. 10.A.5).

Prion amyloid

The next structure we discuss is prion amyloid (2KJ3). Three chains, 79 residues each, form a solenoid which consists of six fragments (two per chain). The shape of the solenoid resembles a double "C", with an outer part and an inner part (Fig. 10.A.6). This amyloid differs from previous examples due to its origin and sequence. What is more, fragments which

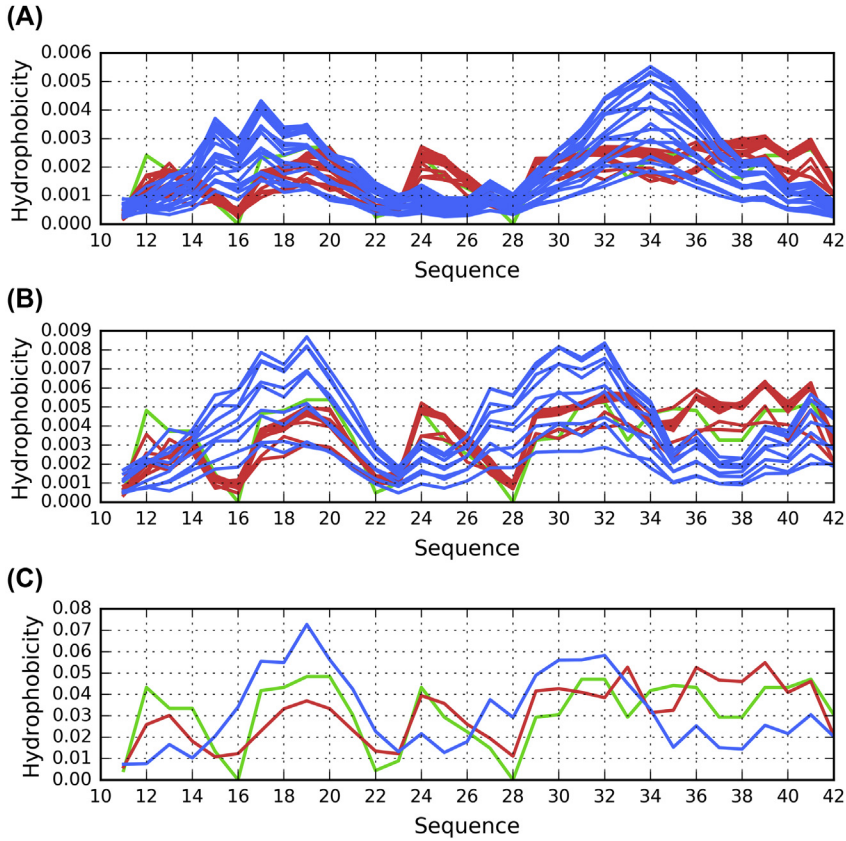

Fig. 10.A.4 Theoretical (T, blue), observed (O, red) and intrinsic (H, green) hydrophobicity distribution profiles for Aβ(11−42) (5KK3). (A) superfibril. (B) protofibril (chains A, B, C, D, E, F, G, H, I). (C) individual (central) chain of protofibril (E). In each case a Gaussian capsule is constructed specifically for the structural unit undergoing analysis.

form the amyloid fibril are not sequentially identical (the sequence of outer "C" differs from the sequence of inner "C"). Note that while amyloids constructed from identical fragments enable rapid clustering of local maxima and minima, the same is not necessarily true for structures which comprise different local sequences.

Linear propagation of alternating hydrophobicity bands appears to be an obvious consequence of alignment of identical fragments, however, in the presented case, the underlying mechanism is somewhat different. Within the solenoid each pair of adjacent twists is formed by two distinct fragments which do not share the same sequence. Aβ(11−42) (2KJ3) therefore appears to be an interesting case study, showing how the formation of alternating bands may occur even in the absence of sequential identity.

Table 10.A.2 Fuzzy oil drop parameters for 5KK3, computed for superfibril, protofibril and chain E, both as a standalone structure, as part of the protofibril and as part of the superfibril. Values given in bold represent the status interpreted as amyloid seed. Values underlined distinguish the status close to amyloid-like expressing significant bias with very high correlation coefficient for HvO relation.

Aβ(11−42) (5KK3)	Fragment	RD		Correlation coefficient		
		T-O-R	T-O-H	HvT	TvO	HvO
Superfibril		0.620	0.534	0.330	0.440	0.756
Protofibril		0.608	0.622	0.235	0.335	0.750
Chain E						
Superfibril		0.565	0.594	0.395	0.466	0.782
Protofibril I		0.569	0.600	0.299	0.286	0.784
Individual E		0.660	0.555	0.355	0.263	0.698
Chain E in superfibril						
Complete	11−42	0.565	0.595	0.396	0.467	0.783
	11−16	0.514	0.296	−0.382	0.265	0.651
	17−23	0.225	0.416	0.826	0.811	0.988
	24−28	**0.575**	0.454	**−0.050**	**−0.215**	**0.982**
	29−35	0.964	0.708	0.423	0.487	0.119
	36−42	0.774	0.784	0.060	0.522	0.530
Chain E in protofibril						
Complete	11−42	0.570	0.601	0.300	0.286	0.784
	11−16	0.538	0.302	−0.376	0.057	0.762
	17−23	0.088	0.189	0.952	0.952	0.986
	24−28	**0.715**	**0.607**	**−0.774**	**−0.872**	**0.982**
	29−35	0.789	0.447	−0.193	0.799	−0.217
	36−42	0.741	0.813	0.647	0.064	0.687
Chain E as individual unit						
Complete	11−42	0.660	0.555	0.356	0.263	0.699
	11−16	0.714	0.345	−0.572	−0.191	0.850
	17−23	0.187	0.193	0.951	0.932	0.931
	24−28	**0.752**	0.410	**−0.556**	**−0.683**	**0.976**
	29−35	0.798	0.478	−0.156	0.526	−0.637

On the other hand, the presented amyloid also presents a significant drawback − from the point of view of our study − namely, it is very short, consisting of only three chains (i.e. six solenoid folds). Under these conditions it is difficult to obtain proof of unrestricted propagation given that

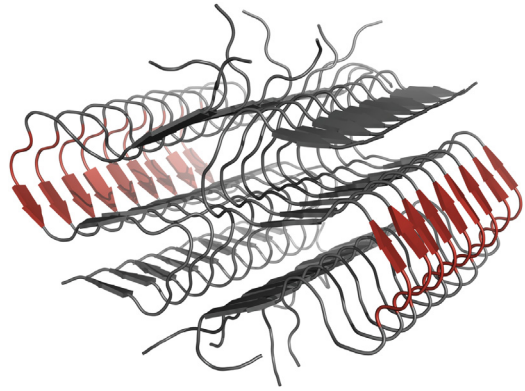

Fig. 10.A.5 3D presentation of Aβ(11—42) (5KK3), with 24—28 fragment highlighted in red.

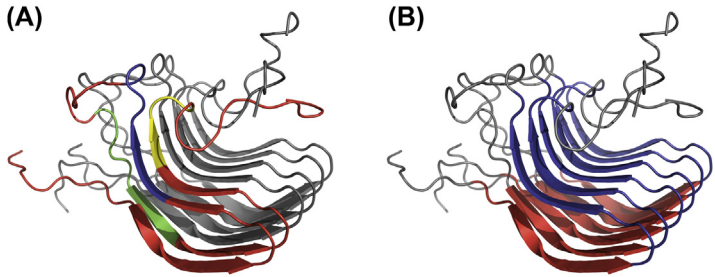

Fig. 10.A.6 3D presentation of prion amyloid (2KJ3). (A) example chain distinguished from the rest of the complex by colors: blue — fragment 241—249, green — fragment 257—264, yellow — fragment 279—283 (rest of the chain is shown in red). (B) solenoid: outer "C" shown in red (fragments 224—235, 261—271 of every chain) and inner "C" shown in blue (fragments 235—246, 271—283 of every chain).

the only non-outlying position is occupied by chain (B) Consequently, RD parameters calculated in this instance (Table 10.A.3) are somewhat less unequivocal than in our previous examples. While intrinsic hydrophobicity is clearly the driving force, shaping the tertiary conformation of 2KJ3 (note the high value of HvO), the solenoid itself is accordant with the theoretical distribution of hydrophobicity — which would suggest the presence of a monocentric hydrophobic core (Fig. 10.A.7).

Table 10.A.3 Fuzzy oil drop parameters for prion amyloid (2KJ3), computed for fibril, chains (treated as part of the fibril) and their fragments. Values given in bold represent the status interpreted as amyloid seed. Values underlined – status of near amyloid form due to the biased relation of correlation coefficients.

Prion amyloid (2KJ3)	Fragment	RD		Correlation coefficient		
		T-O-R	T-O-H	HvT	TvO	HvO
Fibril		0.535	0.411	0.143	0.555	0.615
Chains in fibrl						
Chain A		0.564	0.437	0.101	0.427	0.585
Chain B		0.485	0.368	0.149	0.606	0.615
Chain C		0.534	0.402	0.200	0.592	0.665
Solenoid						
Chain A + B + C	224–246 + 261–283	0.442	0.373	0.373	0.706	0.743
Chain A	241–249	0.846	0.725	−0.047	−0.261	0.340
	257–264	**0.649**	**0.700**	**−0.378**	**−0.410**	**0.781**
	279–283	0.513	0.047	0.645	−0.947	−0.658
Chain B	241–249	0.787	0.730	0.066	0.451	0.662
	257–264	0.652	0.464	-0.106	−0.466	0.612
	279–283	**0.803**	0.346	**-0.688**	**−0.940**	**0.893**
Chain C	241–249	0.836	0.808	0.149	0.417	0.723
	257–264	0.461	0.453	0.174	0.350	0.581
	279–283	**0.864**	0.291	**−0.684**	**−0.952**	**0.578**

The hydrophobicity distribution plots (Fig. 10.A.7) reveal differentiation of individual chains, which is caused by the small size of the amyloid (limited to only three chains). Highlighted fragments deviate from the theoretical distribution in a similar way to our previous examples (i.e. they remain in "active" opposition to T). Much like other proteins discussed in this chapter, 2KJ3 includes "breakers" between strongly hydrophobic bands, and presents local maxima where T expects hydrophobicity to remain low. All these effects counteract the formation of a shared hydrophobic core.

When considering the complex as a whole, the computed value of RD indicates that O remains consistent with T. This, however, may be attributed to the small size of the molecule, as well as to loose fragments which mediate contact with the environment and are capable of adopting a micellar pattern. As shown in Table 10.A.3, individual fragments (in each of the three chains) clearly exhibit amyloid-like properties. This is particularly true for

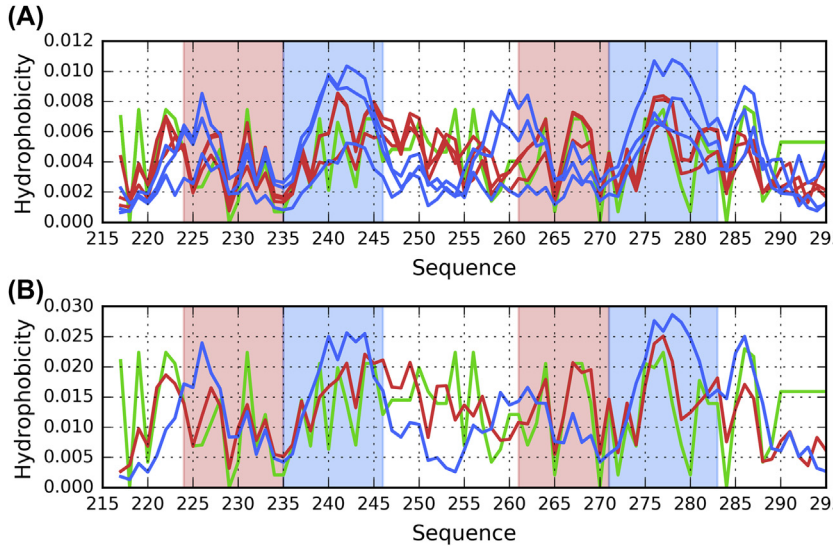

Fig. 10.A.7 Theoretical (T, blue), observed (O, red) and intrinsic (H, green) hydrophobicity distribution profiles for prion amyloid (2KJ3). (A) fibril. (B) chain B (central). In each case a Gaussian capsule is constructed specifically for the structural unit undergoing analysis. Background colors mark the locations of solenoid components: outer "C" (red - fragments 224-235, 261-271) and inner "C" (blue - fragments 235-246, 271-283).

the fragment at 279—283. There is also a notable tendency for bands of high and low hydrophobicity to propagate in an alternating fashion (Fig. 10.A.8).

Fig. 10.A.8 reveals bands of hydrophobicity which emerge despite sequential differences. Notably, local maxima are separated by a deep minimum in each fragment and individual fragments remain in closeness, proximity to one another even though their sequences are not identical. The residue at position 6 in each profile (position in the common regularly ordered fragments) provides a characteristic "breaker" (position 243 and 280), splitting the expected local maximum into two smaller maxima, in a manner similar to Aβ(1—40) (2MVX). This band of low hydrophobicity enables the structure to propagate in a linear manner, thereby "actively" opposing the expected distribution. The effect is not local in scope, but instead dominates the entire fibril. The role of hydrophobicity in amyloid formation is underscored by the observation that only hydrophobic forces may cause tight clustering of strongly charged residues — in contrast to electrostatic interactions which disfavor such structural alignment.

When analyzing the observed distributions we may note that local maxima appearing in successive fragments of the chain differ in amplitude (Fig. 10.A.9). This effect is caused by differences in the sequences of individual fragments; however it does not override the overall conformational

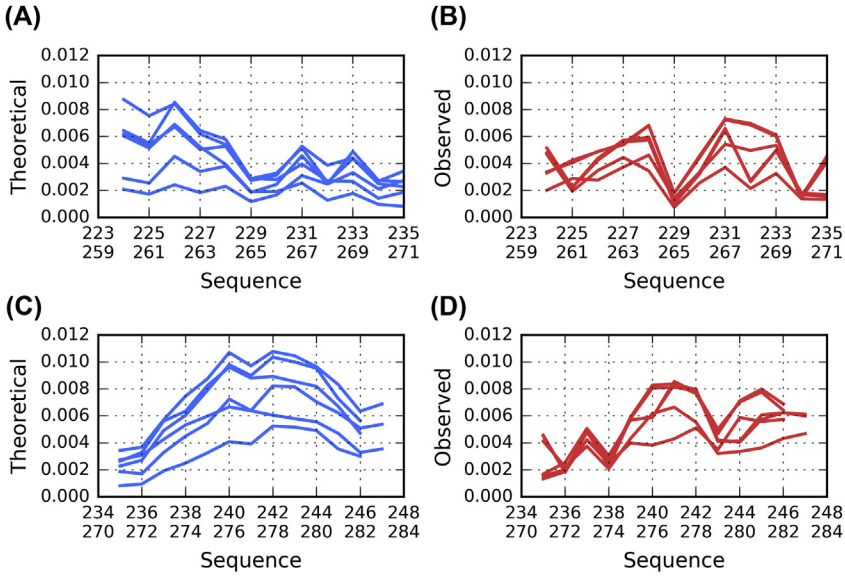

Fig. 10.A.8 Theoretical (T, blue) and observed (O, red) hydrophobicity distribution profiles for prion protein (2KJ3) fragments comprising the solenoid. (A) theoretical distribution in outer "C" (fragments 224—235, 261—271). (B) observed distribution in outer "C" (fragments 224—235, 261—271). (C) theoretical distribution in inner "C" (fragments 235—246, 271—283). (D) observed distribution in inner "C" (fragments 235—246, 271—283).

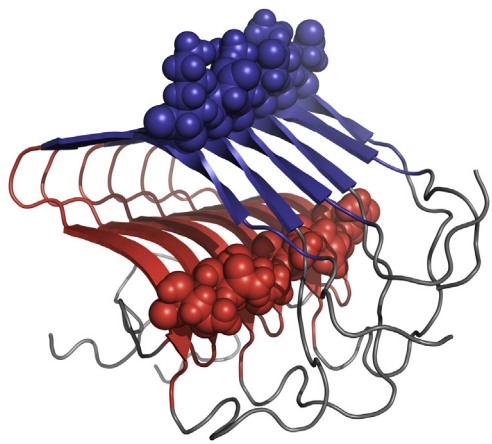

Fig. 10.A.9 3D presentation of prion amyloid (2KJ3) distinguishing fragments 224—235, 261—271 (blue) and 235—246, 271—283 (red). Spheres highlight the positions of residues 229, 265 (blue) and 243, 279 (red).

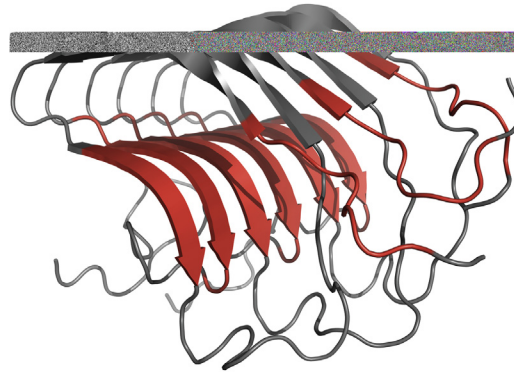

Fig. 10.A.10 3D presentation of prion amyloid (2KJ3) showing fragments which satisfy the proposed amyloid identification criteria. The fragments distinguished as red were identified using the criteria: negative correlation coefficients for HvT and TvO relations accompanied by high values for HvO relation. These fragments are as follows: chain A – 219–226, 239–245, 273–282; chain B – 219–226, 237–245, 273–282; chain C – 219–226, 237–245, 276–282.

pattern, where two local maxima and – even more importantly – the interposing local minimum propagate in a linear fashion.

Comparing T and O distributions for the listed fragments reveals significant differences. While replication of local minima and maxima is not as evident as in the case of Aβ(1–42), the tendency is nevertheless clear and pervades the structure of the amyloid.

As already noted, the limited length of 2KJ3 conceals its fibrillary properties (unlike in previously discussed amyloids which involve greater numbers of individual chains).

Fig. 10.A.10 shows that some of the fragments which exhibit negative correlation coefficients (5 aa moving frame analysis) including also these which do not contribute to the solenoid. In summary, it should be noted that detection and characterization of amyloid structures may be based on parameters provided by the fuzzy oil drop model – in particular, high values of RD (in both variants – T-O-R and T-O-H), negative values of HvT and TvO, along with high values of HvO. These conditions are exemplified by various amyloids listed in PDB, including Aβ(1–40) (2MXU), Aβ(15–40) (2MPZ) [4] and the tau amyloid [5]. It therefore seems justifiable to extend our conclusions to other amyloid structures.

If we accept the premise that the proposed criteria unambiguously categorize certain protein structures as amyloid-like, the following conclusion can be formulated: The amyloid is nothing more than a

micelle – specifically, a ribbonlike micelle. Much like a spherical micelle, the ribbonlike micelle is a self-determining form. If the conformation of the initial chain in the sequence is known with precision, the structure of all subsequent chains may easily be computed. This deterministic property means that, as a whole, the ribbonlike amyloid carries no additional information, regardless of its length.

In silico experiment

In order to assess the ability of the Aβ(1–40) (2MVX) to adopt other conformations, an *in silico* experiment was performed. The polypeptide was subjected to folding simulations using Robetta [6,7] and I-Tasser [8,9], recognized as the most accurate in recent editions of the CASP challenge [10]. The experiment also involved a FOD-based simulation which promotes the formation of a monocentric hydrophobic core and therefore presents an interesting alternative to approaches which do not acknowledge hydrophobic effects [11,12].

Results of the experiment are presented and discussed in Chapter 10.B.

References

[1] Schütz AK, Vagt T, Huber M, Ovchinnikova OY, Cadalbert R, Wall J, Meier BH. Atomic-resolution three-dimensional structure of amyloid β fibrils bearing the Osaka mutation. Angewandte Chemie International Edition 2014;54(1):331–5. https://doi.org/10.1002/anie.201408598.

[2] Colvin MT, Silvers R, Ni QZ, Can TV, Sergeyev I, Rosay M, Griffin RG. Atomic resolution structure of monomorphic Aβ42 amyloid fibrils. Journal of the American Chemical Society 2016;138(30):9663–74. https://doi.org/10.1021/jacs.6b05129.

[3] Van Melckebeke H, Wasmer C, Lange A, Eliso AB, Loquet A, Bockmann A, Meier BH. Atomic-resolution three-dimensional structure of HET-s(218–289) amyloid fibrils by solid-state NMR spectroscopy. Journal of the American Chemical Society 2010;132(39):13765–75. https://doi.org/10.1021/ja104213j.

[4] Dułak D, Banach M, Gadzała M, Konieczny L, Roterman I. Structural analysis of the Aβ(15–40) amyloid fibril based on hydrophobicity distribution. Acta Biochimica Polonica 2018. https://doi.org/10.18388/abp.2018_2647.

[5] Dułak D, Gadzała M, Banach M, Ptak M, Wiśniowski Z, Konieczny L, Roterman I. Filamentous aggregates of tau proteins fulfil standard amyloid criteria provided by the fuzzy oil drop (FOD) model. International Journal of Molecular Sciences 2018;19(10):2910. https://doi.org/10.3390/ijms19102910.

[6] Kim DE, Chivian D, Baker D. Protein structure prediction and analysis using the Robetta server. Nucleic Acids Research 2004;32(Web Server):W526–31. https://doi.org/10.1093/nar/gkh468.

[7] http://robetta.bakerlab.org.

[8] Zhang Y. I-TASSER server for protein 3D structure prediction. BMC Bioinformatics 2008;9(1):40. https://doi.org/10.1186/1471-2105-9-40.

[9] https://zhanglab.ccmb.med.umich.edu/I-TASSER.

[10] http://predictioncenter.org.
[11] Fitzpatrick AWP, Falcon B, He S, Murzin AG, Murshudov G, Garringer HJ, Scheres SHW. Cryo-EM structures of tau filaments from Alzheimer's disease. Nature 2017;547(7662):185–90. https://doi.org/10.1038/nature23002.
[12] Banach M, Konieczny L, Roterman I. Fuzzy oil drop model application—from globular proteins to amyloids. Computational Methods to Study the Structure and Dynamics of Biomolecules and Biomolecular Processes 2018:639–58. https://doi.org/10.1007/978-3-319-95843-9_19.